Chinese Chemical Letters 35 (2024) 108755

Contents lists available at ScienceDirect

Chinese Chemical Letters

journal homepage: www.elsevier.com/locate/cclet

PEG400-mediated nanocarriers improve the delivery and therapeutic efficiency of mRNA tumor vaccines

Wen Xiao[a,1], Fazhan Wang[a,b,1], Yangzhuo Gu[a,1], Xi He[a,1], Na Fan[a], Qian Zheng[a], Shugang Qin[a], Zhongshan He[a], Yuquan Wei[a,*], Xiangrong Song[a,*]

[a] Department of Critical Care Medicine, Frontiers Science Center for Disease-related Molecular Network, State Key Laboratory of Biotherapy, West China Hospital, Sichuan University, Chengdu 610041, China
[b] Medical Research Center, The First Affiliated Hospital of Zhengzhou University, Zhengzhou University, Zhengzhou 450000, China

ARTICLE INFO

Article history:
Received 19 April 2023
Revised 21 June 2023
Accepted 30 June 2023
Available online 3 July 2023

Keywords:
Cancer immunotherapy
mRNA vaccines
DC-targeted delivery
PEGylated liposomes
Cellular uptake

ABSTRACT

Dendritic cell (DC)-targeted delivery of mRNA is a prominent method to boost the efficacy of mRNA tumor vaccines. The targeting ligands are often modified on nanocarriers by polyethylene glycol (PEG) linker in mRNA delivery systems. Whether the PEG linker length influences the targeting delivery efficiency of mRNA nanocarrier *in vivo* remains unclear. Here, we designed and constructed DC-targeted mRNA delivery systems modified by mannose *via* different PEG linker lengths (100/400/1000/2000) (MP_n-LPX). The top candidate MP_{400}-LPX (the linker was PEG400) showed the optimal mRNA expression and antigen presentation owing to the highly efficient uptake by DCs. Furthermore, MP_{400}-LPX could better inhibited tumor growth and extended survival in the E.G7-OVA lymphoma and TC-1 cervical tumor mouse model. Collectively, these results demonstrated that PEG400 was the optimal linker for the PEGylated DC-targeted mRNA vaccines. Our findings provided a new platform for the rational design of targeted mRNA nanovaccines with shorter-length PEG.

mRNA vaccines against coronavirus disease-19 (COVID-19) have been approved by the Food and Drug Administration (FDA) owing to their unique advantages (*i.e.*, low risk of insertional mutagenesis, short development cycles and easy industrialization) [1–4]. The successful application of mRNA vaccines also brings great hope for tumor immunotherapy [5–7]. However, the anti-tumor efficiency of mRNA vaccines was not so satisfactory. Many aspects, such as mRNA vaccine delivery systems, are eagerly required further optimization and improvement to accelerate the clinical transformation of mRNA vaccines [8–11]. Dendritic cells (DCs) are the major professional antigen-presenting cells (APCs) that play a key role in inducing antigen-specific immune response [12–15]. Therefore, it should be a valuable approach to developing the DC-targeted mRNA delivery systems for improving antigen expression and inducing robust immune responses [16–18].

The targeting ligands are often linked on the surface of nanomedicines by polyethylene glycol (PEG) to achieve the specific targeting, and such strategy is also commonly applied for the DC-targeted mRNA vaccines [19–21]. PEG2000 was widely used as the linker for nanomedicines in these studies without reasonable optimization. However, the PEG length has been studied to significantly influence the delivery of nanomedicines to the target site and the uptake by the specific cells [22–24]. For example, Yamada *et al.* reported that the longer linker PEG5000 might present the targeting ligand more effectively [25]. While Stefanick *et al.* reported that longer PEG may fold into a mushroom shaped spherical structure to bury the conjugated ligand, which was not beneficial for the binding of modified ligands on the nanoparticle to its receptors on the target cell [24,26,27]. Moreover, our previous study found that PEG1000 was better than PEG2000 as the linker of mannose-conjugated liposomes for mRNA delivery to DCs *in vitro* [21]. Hence, it could be hypothesized that the mannose-conjugated liposomes with optimal linker length might induce powerful anti-tumor immune response of mRNA vaccines *in vivo*.

In this study, we aimed to enhance the mRNA delivery efficiency of DCs *via* further optimization of PEG linker length, thereby improving the anti-tumor efficacy of mRNA vaccines *in vivo*. All animal experiments were approved by the Animal Experimental Ethics Committee of the State Key Laboratory of Biotherapy of Sichuan University. As shown in Fig. 1, mannose, one of the classic target ligands for DCs, was selected as the model ligand. It was conjugated to cholesterol *via* PEG with different linker length

* Corresponding authors.
E-mail addresses: yqwei@scu.edu.cn (Y. Wei), songxr@scu.edu.cn (X. Song).
[1] These authors contributed equally to this work.

https://doi.org/10.1016/j.cclet.2023.108755
1001-8417/

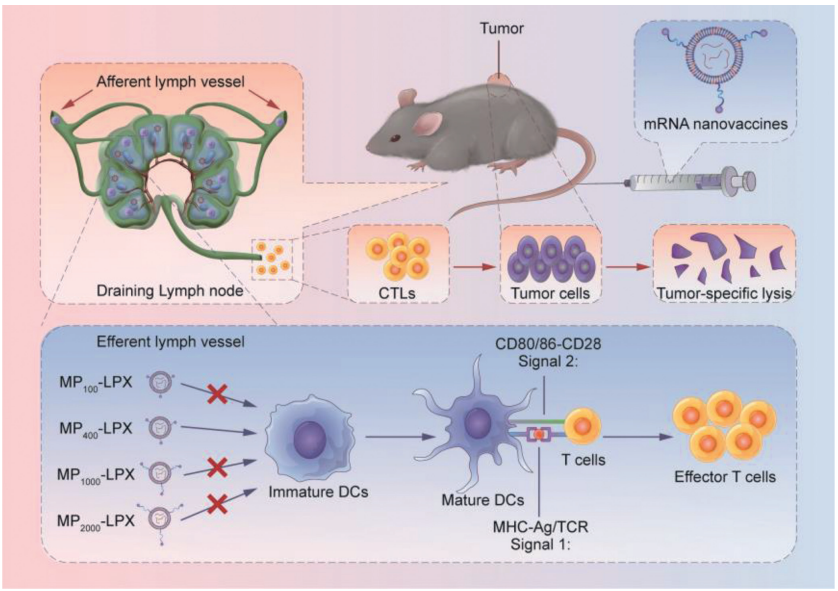

Fig. 1. Schematic diagram of MP_n-LPX targeting to DCs for potent cancer immunotherapy. LPX decorated with MP_{400}-CH had optimal target ability to DCs owing to the maximum exposure of mannose. MP_{400}-LPX exerted the best antigen presentation efficiency and therapeutic cancer immune protection efficacy among MP_{100}-LPX, MP_{1000}-LPX and MP_{2000}-LPX *in vivo*.

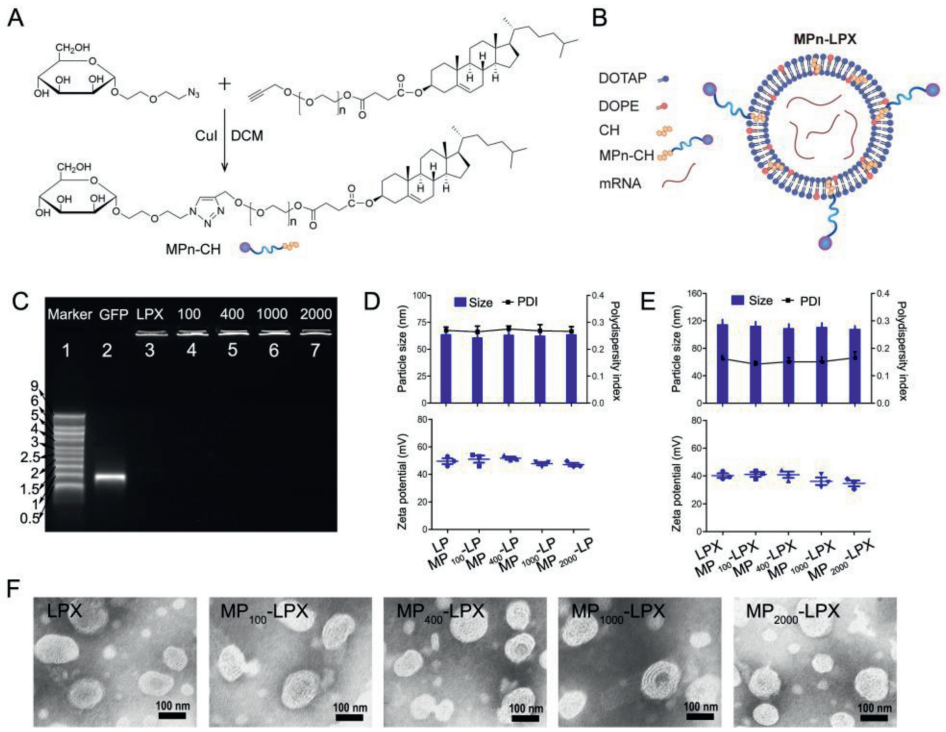

Fig. 2. Preparation and characterization of MP_n-LPX. (A) Schematic of the synthetic steps for MP_n-CH. The number of ethylene glycol unit (n) in MP_{100}-CH, MP_{400}-CH, MP_{1000}-CH, and MP_{2000}-CH are 0, 9, 22, and 45, respectively. (B) Schematic structure of MP_n-LPX. (C) Gel electrophoresis retardation assay of MP_n-LPX. Marker (Marker, lane 1), free GFP-mRNA (GFP, lane 2), LPX (LPX, lane 3), MP_{100}-LPX (100, lane 4), MP_{400}-LPX (400, lane 5), MP_{1000}-LPX (1000, lane 6) and MP_{2000}-LPX (2000, lane 7). (D, E) Size, polydispersity index and zeta potential of MP_n-LP (D) and MP_n-LPX (E) ($n = 3$). (F) TEM images of MP_n-LPX with different PEG linker lengths. Scale bar: 100 nm. Error bars indicate mean ± standard error of mean (SEM).

(100/400/1000/2000). The obtained mannose-cholesterol conjugates (MP_n-CH) were then applied to construct the DC-targeted mRNA tumor vaccines (MP_n-LPX). The cellular uptake, mRNA expression and anti-tumor therapeutic efficacy were systematically investigated. We reported that PEG400 was the optimal PEG linker length for DC-targeted mRNA vaccine delivery to induce a potent anti-tumor immunogenicity, which would provide key features for the design of PEGylated mRNA nanoparticles and other PEGylated targeting nanomedicines.

The mannose receptor (CD206) overexpressed on DCs is an ideal candidate target for the DC-targeted design of vaccines [28–30]. Then mannose was selected as a model ligand to prepare DC-targeted mRNA vaccines in this study. Firstly, mannose was coupled to cholesterol with different PEG linker lengths (100/400/1000/2000) to obtain MP_n-CH (Fig. 2A). Compared to the reported synthesis methods of mannose-modified target materials (such as Man-C4-chol [31] or DSPE-PEG-mannose [32]), we adopted relatively mild esterification and click reaction methods

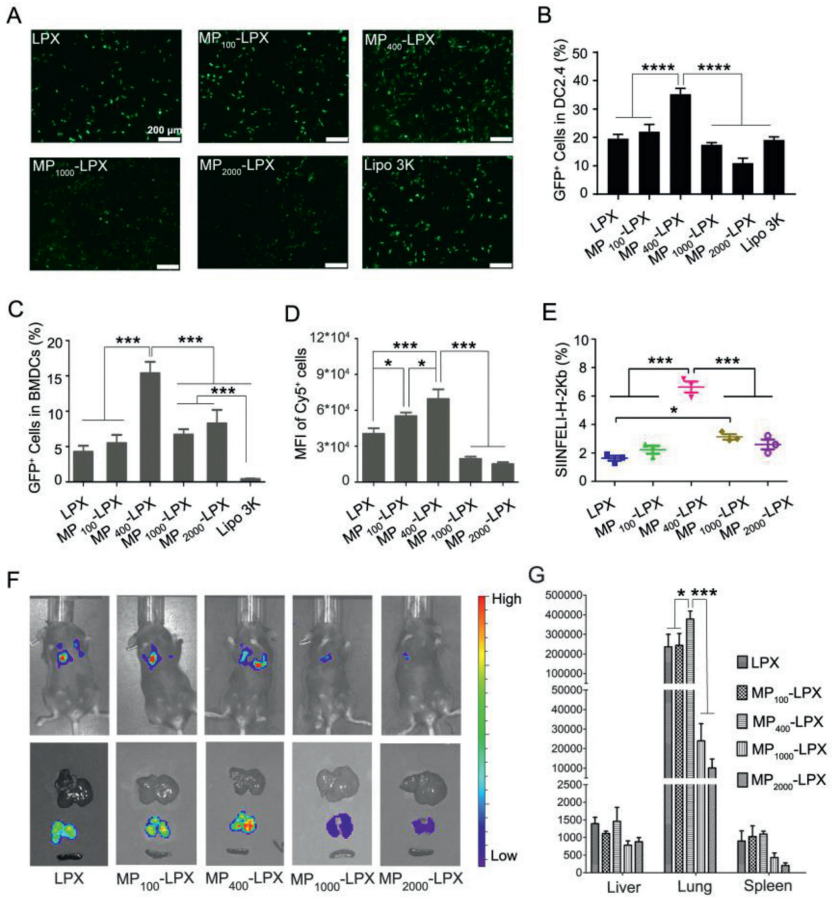

Fig. 3. Effects of MP_n-LPX with different PEG linker lengths on the mRNA delivery efficiency *in vitro* and *in vivo*. (A, B) Transfection capacity of MP_n-LPX carrying GFP-mRNA in DC2.4 cells. (A) GFP expression by DC2.4 cells observed by a fluorescence microscope. Scale bar: 200 μm. (B) Transfection efficiency (% GFP^+ cells) was quantified by flow cytometry ($n = 3$). (C) Transfection efficiency of MP_n-LPX carrying GFP-mRNA on BMDCs ($n = 3$). (D) Cellular uptake of MP_n-LPX carrying Cy5-mRNA in DC2.4 cells ($n = 3$). (E) Antigen presentation of MP_n-LPX carrying OVA-mRNA in BMDCs ($n = 3$). (F) Representative whole body and isolated organs images of C57BL/6 mice demonstrated the mRNA expression 6 h after injection of Luc-mRNA loaded MP_n-LPX. (G) The quantitative fluorescence intensity of Luc-mRNA expression in liver, lung and spleen ($n = 3$). Error bars indicate mean ± SEM. Statistical analysis was performed using a one-way ANOVA comparison. $^*P < 0.05$, $^{***}P < 0.001$, $^{****}P < 0.0001$.

to synthesize MP_{400}-CH in our previous work (Fig. S1A in Supporting information) [21], which had the advantages of simple and easy scale-up production. Finally, MP_{100}-CH, MP_{400}-CH, MP_{1000}-CH and MP_{2000}-CH were obtained with yields of 68.6%, 66.8%, 56.9% and 47.9%, respectively. Besides, P_{400}-CH without mannose modification was also reasonable designed and acquired (Fig. S1B in Supporting information). The product of MP_{400}-CH was confirmed by ^{1}H-nuclear magnetic resonance (^{1}HNMR), electrospray ionization-tandem mass spectrometry (ESI-MS), Fourier transform infrared (FTIR) and high-performance liquid (HPLC), respectively (Fig. S2 in Supporting information). The structure of P_{400}-CH was also confirmed with the purity of 98.203% by ^{1}HNMR and HPLC (Fig. S3 in Supporting information).

The cationic liposomes have been used for mRNA delivery both preclinical and in clinical trial [33,34]. Next, cationic liposomes consisting of DOTAP and cholesterol (Shanghai A.V.T. Pharmaceutical Co., Ltd.) were modified by MP_n-CH (MP_n-LPs) were prepared by film hydration method for further study. mRNA-complexed mannose-modified liposomes (MP_n-LPX) were obtained by mixing MP_n-LPs with mRNA (Fig. 2B). The complete complexation of mRNA with MP_{400}-LPs was confirmed by gel electrophoresis when the N/P ratio of 3 (Fig. S4 in Supporting information). We further demonstrated that all MP_n-LPs had good complexation with mRNA at the N/P ratio of 3 by the gel electrophoresis experiment (Fig. 2C). The particle size of all different MP_n-LPX was approximate 110 nm and the PDI was less than 0.2 (Fig. 2E), while that of MP_n-LPs was about 65 nm and the PDI was less than 0.3 (Fig. 2D). Moreover, zeta potential of MP_n-LPX (~40 mV) was slightly lower than MP_n-LPs (~50 mV) due to the successful complexation of mRNA (Figs. 2D and E). The diluted MP_n-LPX and MP_n-LPs were both colorless and transparent, which had significant Tyndall effect (Fig. S5 in Supporting information). The transmission electron microscopy (TEM) also revealed that MP_n-LPX was spherical with a distinct lipid membrane structure (Fig. 2F). Besides, the storage stability of the MP_n-LPX was investigated by observing the change of size, zeta potential and mRNA leakage. The results showed that the particle size, zeta potential and mRNA leakage did not decrease significantly after storage, confirming the excellent storage stability of MP_n-LPX (Figs. S6 and S7 in Supporting information). Collectively, different linker lengths of PEG did not affect particle size, surface charge, appearance, Tyndall effect and micromorphology of MP_n-LPX.

Although different PEG linker lengths did not affect the characterization of MP_n-LPX based on the above results, whether it affected the mRNA delivery efficiency needed to be further investigated. Therefore, the mRNA encoding green fluorescent protein (GFP) was used to evaluate the *in vitro* transfection efficiency of MP_n-LPX in DC2.4 cells and bone marrow-derived dendritic cells (BMDCs). The expression rates of CD206 on DC2.4 cells and BMDCs were about 35% and 23% by flow cytometry (Fig. S8 in Supporting information), indicating that these cells could be used to investigate the targeted delivery ability of MP_n-LPX. Firstly, GFP ex-

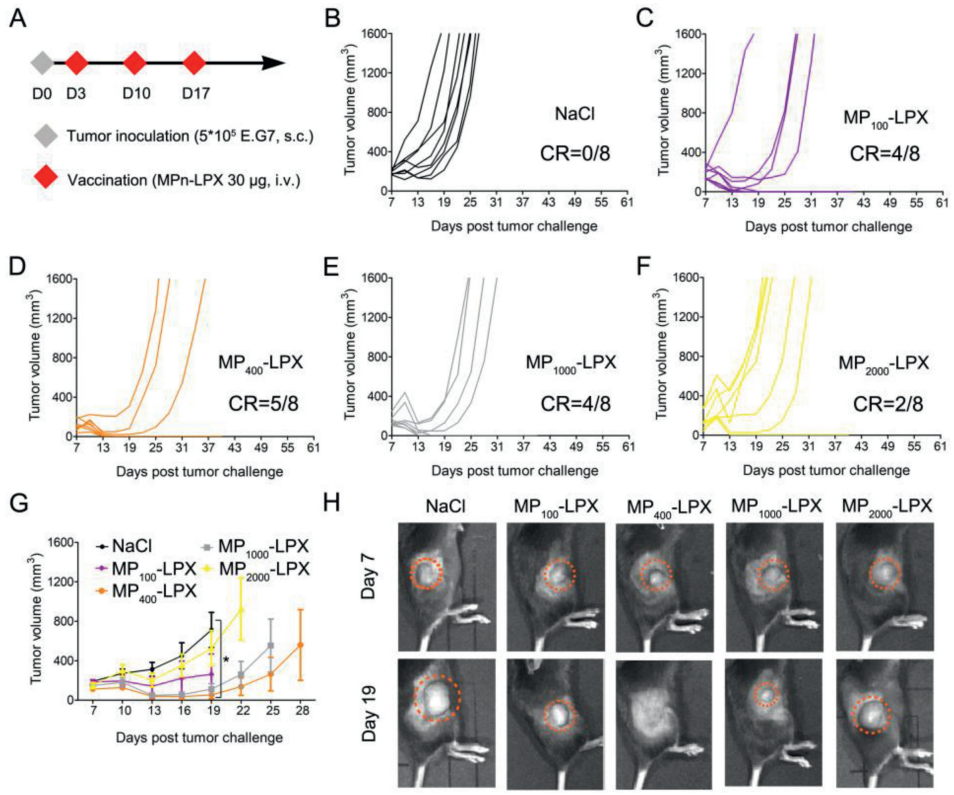

Fig. 4. Antitumor effect of MP_n-LPX in the E.G7 murine tumor model. (A) Experimental setup of the therapeutic immunization. (B–F) Individual tumor growth curve of each mouse. (G) Average tumor growth curves in each group ($n = 8$ mice per group). (H) Representative images of tumor size on day 7 and day 19. Error bars indicate mean ± SEM. Statistical analysis was performed using a one-way ANOVA comparison. $^*P < 0.05$.

pression in DC2.4 cells was observed by fluorescence microscope (Fig. 3A), and was quantitatively analyzed by flow cytometry. The mRNA transfection efficiency of MP_{400}-LPX was up to 40%, which was significantly higher than other groups in DC2.4 cells (Fig. 3B). The transfection ability of P_n-LPX without mannose modification on DC2.4 cells was also investigated. As shown in Fig. S9 (Supporting information), the transfection efficiency of P_{1000}-LPX and P_{2000}-LPX with longer PEG length was lower than that of P_{400}-LPX with shorter PEG length. Moreover, the targeting effect of mannose significantly enhanced the transfection efficiency of MP_{400}-LPX, compared with P_{400}-LPX. Meanwhile, the transfection stability of MP_{400}-LPX on DC2.4 cells was investigated. As shown in Fig. S10 (Supporting information), the transfection efficiency remained stable when MP_{400}-LPX was placed at 4 °C for 10 days. The transfection efficiency decreased significantly when stored for 15 days, suggesting that although MP_{400}-LPX exerted no significantly change in particle size and potential at 4 °C, the active component mRNA may have been degraded at day 15. Overall, MP_{400}-LPX could remain the biological function at 4 °C for at least 10 days.

Similarly, GFP expression in MP_n-LPX treated BMDCs was measured, and the represent scatter diagram of each condition was shown in Fig. S11 (Supporting information). As shown in Fig. 3C, MP_{400}-LPX (15.03% ± 2.11%) exerted the highest transfection efficiency compared with LPX (4.25% ± 0.86%), MP_{100}-LPX (5.48% ± 1.16%), MP_{1000}-LPX (6.67% ± 0.79%) and MP_{2000}-LPX (7.59% ± 3.02%). Collectively, MP_{400}-LPX has the best mRNA delivery efficiency in DCs, even better than MP_{2000}-LPX and MP_{1000}-LPX.

In order to explore why MP_{400}-LPX could perform better in delivering mRNA for expression, we further investigated the targeting recognition ability of MP_n-LPX to DCs by cellular uptake assay. MP_n-LPX loaded Cy5 mRNA was used to study cellular uptake in DC2.4 cells by flow cytometry. Firstly, 6 h was selected as the time point for the cellular uptake of MP_n-LPX, because the most uptake of MP_{400}-LPX was seen at the incubation time of 6 h in the preliminary experiment (Fig. S12 in Supporting information). When the DC2.4 cells were treated with MP_n-LPX for 6 h, almost all of the cells were Cy5-positive (>98%) (Fig. S13 in Supporting information). Surprisingly, MP_{400}-LPX treated DC2.4 cells exhibited the highest mean fluorescence intensity (MFI) of Cy5-positive cells among different groups (Fig. 3D). Furthermore, the uptake blocking experiment by mannose was further conducted in DC2.4 cells to verify the targeted delivery potency of MP_{400}-LPX (Fig. S14 in Supporting information). These results were consistent with previous reports that short alkyl chains may be more flexible and easier to interact with cellular lipid membranes. While longer alkyl chains may face the energetic barrier when inserting into cell membrane, slowing down the endocytosis process of nanoparticle [35]. Moreover, the delivery efficiency was further improved with the introduction of mannose-target head. Collectively, those results revealed that PEG400 may be the optimal linker length for the exposure of the targeting ligand for receptor recognition, while the longer linker (PEG1000 and PEG2000) might bury the conjugated ligand to decrease the cellular uptake, thus MP_{400}-LPX exerted the highest cellular uptake and transfection efficiency.

Efficient antigen presentation by APCs is the prerequisite for the high efficacy of mRNA vaccines [36]. Therefore, the antigen presentation ability of MP_n-LPX treated BMDCs was further detected by loading ovalbumin (OVA)-mRNA. Significant antigen-presentation of the OVA peptide SIINFEKL was observed in MP_{400}-LPX treated BMDCs (Fig. 3E). This result indicated that MP_{400}-LPX treated BMDCs had the optimal antigen presentation due to the maximum mRNA expression, which would be more conducive for the activation of antigen-specific T cell immune response to realize tumor immunotherapy *in vivo*. Moreover, the co-stimulatory signals pro-

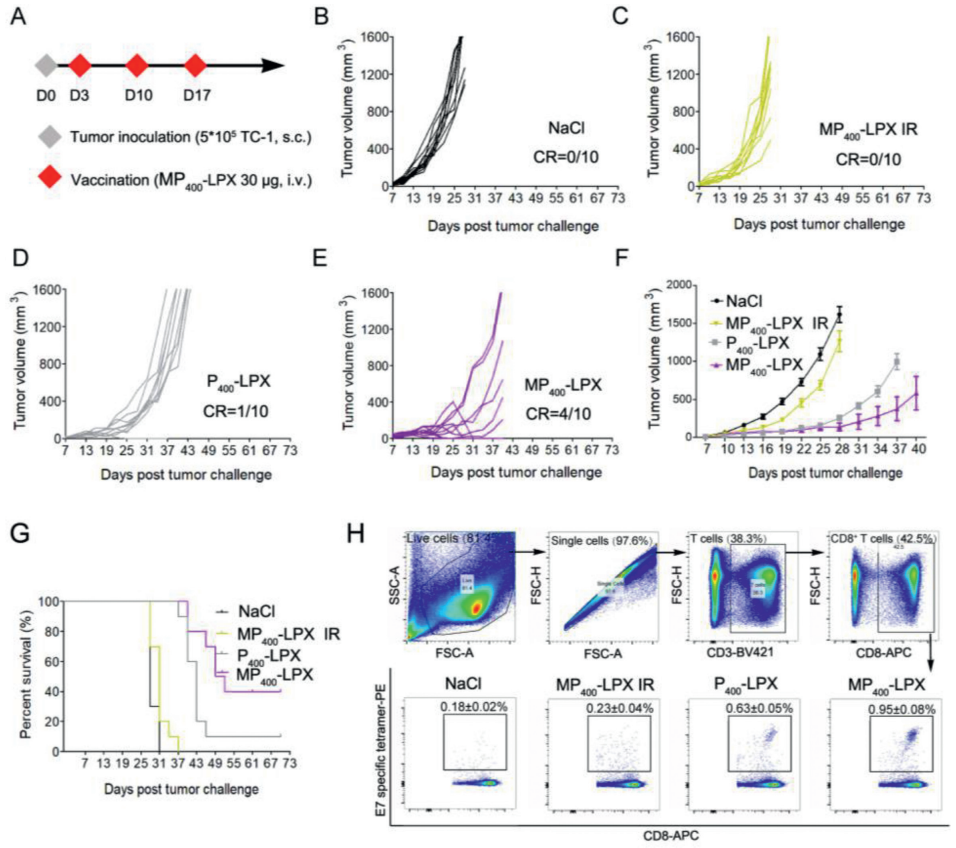

Fig. 5. Therapeutic effect of MP_{400}-LPX in the TC-1 tumor model. (A) Experimental setup of the therapeutic immunization. C57BL/6 mice were inoculated subcutaneously with 5×10^5 TC-1 tumor cells on day 0. On days 3, 10, and 17, tumor-bearing mice were treated with indicated formulations containing 30 μg/dose of mRNA. (B–E) Individual tumor growth curves. (F) Average tumor growth curves. (G) Survival curves of each group ($n = 10$ mice per group). (H) MP_{400}-LPX induced significantly enhanced E7-specific $CD8^+$ T cell responses than P_{400}-LPX ($n = 3$). The data are shown as mean ± SEM.

vided by matured DCs are also need for T cell activation. As shown in the Fig. S15 (Supporting information), the proportion of $CD86^+$ cells in $CD11c^+$ BMDCs treated with MP_n-LPX loaded with OVA mRNA increased significantly, compared with the untreated control group. These results indicate that MP_n-LPX vaccine could effectively promote the maturation of DCs. However, different PEG chain length does not affect the ability of MP_n-LPX to activate DCs.

Next, we explored the mRNA expression of MP_n-LPX *in vivo*. C57BL/6 mice were administered MP_n-LPX encapsulating luciferase-encoding mRNA (Luc-mRNA) intravenously. The whole body and the isolated organs images of the injected mice were captured with IVIS systems and representative images were shown in Fig. 3F. Consistent with *in vitro* transfection results, the expression of Luc-mRNA in lung tissues of mice in MP_{400}-LPX group was obviously the best. To further quantify the expression of the Luc-mRNA in specific organs, the average fluorescence signal in lungs, spleen and liver were quantified (Fig. 3G). MP_{400}-LPX induced stronger Luc-mRNA expression in the lung site compared with LPX, MP_{100}-LPX, MP_{1000}-LPX and MP_{2000}-LPX *in vivo*. Of note, DOTAP cationic liposomes (N/P = 3) were predominantly distributed in the lungs, which are equipped with an immune defense mechanism that involves a large number of DCs that can present antigens to T cells [37,38]. The strongest expression of PEG400-mediated MP_{400}-LPX in the lung might be attributed to the targeting effect on DCs in the lungs, thus accumulating more lipoplex for expression in the lung. On the other hand, longer PEG might inhibit the uptake of lipoplex by tissue cells due to "PEG dilemmas" [39]. In conclusion, the superiority of MP_{400}-LPX in delivering mRNA *in vitro* and *in vivo* encourages us to further investigate the antitumor efficacy of MP_n-LPX *in vivo*.

Encouraged by the above results, we further studied the effect of PEG linker length on the immunotherapeutic effect of MP_n-LPX in murine tumor model *in vivo*. Firstly, the therapeutic effect of MP_n-LPX on the EG.7-OVA mouse tumor model was investigated. MP_n-LPX vaccines loaded with OVA mRNA also had good pharmacologic properties (Table S2 in Supporting information). In the current study, immunization was initiated on day 3 when E.G7 tumors were palpable (Fig. 4A). The immunization route of mRNA nanovaccine was preliminarily studied. As shown in Fig. S16 (Supporting information), MP_{400}-LPX induced better anti-tumor efficacy by intravenous administration compared with intraperitoneal or intradermal injection. It has been reported that the antigens are quickly expressed *in vivo* following intravenous administration. This appears to result in a faster generation of specific $CD8^+$ T cells for better therapeutic effects [40]. Besides, intravenous injection is also commonly used in preclinical and clinical trial studies of mRNA tumor vaccines [41,42]. Therefore, intravenous administration was chosen for the immunotherapy evaluation of MP_n-LPX. As shown in Figs. 4B-G, MP_{100}-LPX, MP_{400}-LPX and MP_{1000}-LPX significantly delayed the tumor growth. Surprisingly, the tumor cure rate (CR) of MP_{400}-LPX treated group was 5/8, whereas those in NaCl, MP_{100}-LPX, MP_{1000}-LPX or MP_{2000}-LPX treated group were 0/8, 4/8, 4/8 and 2/8, respectively. Noteworthy, the tumor volume of MP_{400}-LPX-vaccinated mice was smaller than any other groups (Fig. 4H).

Furthermore, we studied the anti-tumor effects of MP_{400}-LPX and P_{400}-LPX in TC-1 murine tumor model to explore the importance of DCs targeting. Similarly, C57BL/6 mice were subcutaneously injected with TC-1 cells to establish TC-1 murine tumor model and then subjected to three intravenous injections with HPV 16 E6/E7 mRNA-loaded vaccines (Fig. 5A). As shown in Figs. 5B–

F, MP_{400}-LPX IR loaded with non-therapeutic mRNA was prepared for administration, which had no inhibitory effect on tumor as the control group given PBS. And MP_{400}-LPX exhibited the better antitumor effect with the tumor CR of 4/10, compared with 1/10 for P_{400}-LPX. Additionally, treatment with MP_{400}-LPX significantly prolonged the survival time of mice compared with P_{400}-LPX (Fig. 5G). In detail, the median survival of MP_{400}-LPX treated mice was 52 days, whereas those of P_{400}-LPX treated mice and NaCl treated mice was 43 days and 28 days, respectively.

Importantly, tumor-specific cytotoxic T lymphocytes (CTLs) were further assessed by flow cytometry. Cell gating strategy was shown in Fig. 5H. The highest percentages of E7-specific $CD8^+$ T cells in the blood of mice immunized with MP_{400}-LPX was observed with the percentages of 0.95% ± 0.08%. The above results indicated that MP_{400}-LPX with PEG400 modified had the best tumor immunotherapy effect, which was consistent with the results of the mRNA delivery efficiency *in vitro*.

Finally, we systematically explored the safety of MP_{400}-LPX. Firstly, cytotoxicity analysis of MP_{400}-LPX was performed by flow cytometry. Data showed that MP_{400}-LPX performed good safety *in vitro* when incubated with DC2.4 cells (Fig. S17 in Supporting information). Moreover, to assay the safety of MP_{400}-LPX mRNA tumor vaccine after intravenous administration, the *in vitro* hemolysis analysis was further performed. No visible hemolytic activity was observed in MP_{400}-LPX, P_{400}-LPX or NaCl treated rabbit red blood cells (Figs. S18A and B in Supporting information), indicating that MP_{400}-LPX might perform good blood compatibility and would be safe for systemic delivery.

While the therapeutic efficacy of the MP_{400}-LPX *in vivo* and good blood compatibility *in vitro* were confirmed, it remains critical to evaluate its safety *in vivo* for its further application. The serological and histopathological analyses were carried out at the end of the tumor immunotherapy evaluation study. No significant effects of MP_{400}-LPX immunization on profile and blood cells were observed (Fig. S18C in Supporting information). Importantly, no significant toxic pathological changes in the heart, liver, spleen, lung, and kidney were identified in MP_{400}-LPX or P_{400}-LPX treated mice (Fig. S18D in Supporting information). These data all confirmed that MP_{400}-LPX had good safety.

In summary, we have investigated the effect of the link length between the target ligand and the nanocarriers on the mRNA delivery efficiency and immunotherapeutic efficacy of DC-targeted mRNA vaccines. Mannose was conjugated to cholesterol *via* PEG with different linker length (100/400/1000/2000) by click reaction to obtain the mannose-cholesterol conjugate (MP_n-CH). MP_n-CH was then successfully applied to construct the DC-targeted mRNA tumor vaccines (MP_n-LPX). Although MP_n-LPX exhibited comparable particle size and zeta potential, MP_{400}-LPX showed the highest mRNA delivery efficiency in DCs. It may be PEG400 was the optimal linker length, which could expose the target ligand enough for receptor recognition, so as to maximize the targeted uptake by DCs. Furthermore, *in vivo* data generated from tumor-bearing mice further demonstrated that MP_{400}-LPX evoked potent antitumor immune responses accompanied by marked inhibition of tumor growth. Overall, our work thus identified the optimal linker length (PEG400) of the ligand for DC-targeted mRNA vaccines, which could also provide certain universal reference for the rational design of nanocarriers with shorter-length PEG.

Declaration of competing interest

The authors declare that they have no known competing financial interests or personal relationships that could have appeared to influence the work reported in this paper.

Acknowledgments

This work was financially supported by National Key S&T Special Projects (No. 2018ZX09201018–024), Henan Medical Science and Technology Joint Building Program (No. SBGJ202102132), China Postdoctoral Science Foundation (No. 2020TQ0282), Henan Province Youth Talent Promoting Project (No. 2022HYTP047), Key Research and Development Project of Henan Province (No. 232102311224) and Sichuan Provincial Science and Technology Innovation (Seedling Project) Cultivation Projects (No. MZGC20230034). Thanks are given to the Home for Researchers (https://www.home-for-researchers.com) for helping with the scheme.

Supplementary materials

Supplementary material associated with this article can be found, in the online version, at doi:10.1016/j.cclet.2023.108755.

References

[1] U. Elia, S. Rotem, E. Bar-Haim, et al., Nano Lett. 21 (2021) 4774–4779.
[2] F.P. Polack, S.J. Thomas, N. Kitchin, et al., N. Engl. J. Med. 383 (2020) 2603–2615.
[3] K.P. Chen, N. Fan, H. Huang, et al., Adv. Funct. Mater. 32 (2022) 2204692.
[4] Q. Xiong, G.Y. Lee, J. Ding, W. Li, J. Shi, Nano Res. 11 (2018) 5281–5309.
[5] M.A. Islam, J. Rice, E. Reesor, et al., Biomaterials 266 (2021) 120431.
[6] Y.X. Lin, Y. Wang, J. Ding, et al., Sci. Transl. Med. 13 (2021) eaba9772.
[7] S. Qin, X. Tang, Y. Chen, et al., Signal Transduct. Target. Ther. 7 (2022) 166.
[8] R. Kuai, L.J. Ochyl, K.S. Bahjat, et al., Nat. Mater. 16 (2017) 489–496.
[9] Y. Liu, S. Li, S. Lin, et al., Chin. Chem. Lett. 34 (2023) 107987.
[10] X. Duan, Y. Zhang, M. Guo, et al., Acta Pharm. Sin. B 13 (2023) 942–954.
[11] L.J. Kubiatowicz, A. Mohapatra, N. Krishnan, R.H. Fang, L. Zhang, Exploration 2 (2022) 20210217.
[12] Y. Yin, X. Li, H. Ma, et al., Nano Lett. 21 (2021) 2224–2231.
[13] Y. Wu, Z. Zhang, Y. Wei, et al., Chin. Chem. Lett. 34 (2023) 108098.
[14] L. Miao, L. Li, Y. Huang, et al., Nat. Biotechnol. 37 (2019) 1174–1185.
[15] C. Fu, L. Zhou, Q.S. Mi, et al., Cells 11 (2022) 222.
[16] H.J. Kim, S.K. Seo, H.Y. Park, J. Control. Release 345 (2022) 405–416.
[17] L.M. Kranz, M. Diken, H. Haas, et al., Nature 534 (2016) 396–401.
[18] M.A. Oberli, A.M. Reichmuth, J.R. Dorkin, et al., Nano Lett. 17 (2017) 1326–1335.
[19] K. Van der Jeught, S. De Koker, L. Bialkowski, et al., ACS Nano 12 (2018) 9815–9829.
[20] X. Zhuang, Y. Qi, M. Wang, et al., Vaccines 8 (2020) 123.
[21] F. Wang, W. Xiao, M.A. Elbahnasawy, et al., Front. Pharmacol. 9 (2018) 980.
[22] L.J. Cruz, P.J. Tacken, R. Fokkink, et al., Biomaterials 32 (2011) 6791–6803.
[23] H.S. Jeong, K.S. Na, H. Hwang, et al., J. Biomed. Mater. Res. A 102 (2014) 4545–4553.
[24] J.F. Stefanick, J.D. Ashley, T. Kiziltepe, et al., ACS Nano 7 (2013) 2935–2947.
[25] A. Yamada, Y. Taniguchi, K. Kawano, et al., Clin. Cancer Res. 14 (2008) 8161–8168.
[26] C. Allen, N. Dos Santos, R. Gallagher, et al., Biosci. Rep. 22 (2002) 225–250.
[27] N. Dos Santos, C. Allen, A.M. Doppen, et al., Biochim. Biophys. Acta 1768 (2007) 1367–1377.
[28] F. Perche, T. Benvegnu, M. Berchel, et al., Nanomedicine 7 (2011) 445–453.
[29] C. Pichon, P. Midoux, Methods Mol. Biol. 969 (2013) 247–274.
[30] O.V. Markov, N.L. Mironova, E.V. Shmendel, et al., J. Control. Release 213 (2015) 45–56.
[31] C. Lai, S. Duan, F. Ye, et al., Theranostics 8 (2018) 1723–1739.
[32] R. Yang, J. Xu, L. Xu, et al., ACS Nano 12 (2018) 5121–5129.
[33] K.T. Magar, G.F. Boafo, X.T. Li, Z.J. Chen, W. He, Chin. Chem. Lett. 33 (2022) 587–596.
[34] W. Zhang, Y.X. Jiang, Y.L. He, et al., Acta Pharm. Sin. B 13 (2023) 4105–4126.
[35] X. Ke, Z. Wei, Y. Wang, et al., Nanomedicine 19 (2019) 126–135.
[36] A.L. Huff, E.M. Jaffee, N. Zaidi, J. Clin. Invest. 132 (2022) e156211.
[37] P.C. Cook, A.S. MacDonald, Semin. Immunopathol. 38 (2016) 449–460.
[38] T. Kawasaki, M. Ikegawa, T. Kawai, Front. Immunol. 13 (2022) 860915.
[39] S. Zalba, T.L.M. Ten Hagen, C. Burgui, et al., J. Control. Release 351 (2022) 22–36.
[40] L. Fend, T. Gatard-Scheikl, J. Kintz, et al., Cancer Immunol. Res. 2 (2014) 1163–1174.
[41] L. Pan, L. Zhang, W. Deng, et al., J. Control. Release 357 (2023) 133–148.
[42] W. Yang, T. Miyazaki, Y. Nakagawa, et al., Sci. Technol. Adv. Mater. 24 (2023) 2170164.